T. & A. M. Report No. 322

AN EXPERIMENTAL EVALUATION OF PLASTICITY THEORIES FOR ANISOTROPIC METALS

by

R. M. W. Frederking and O. M. Sidebottom

Department of Theoretical and Applied Mechanics
University of Illinois

April 1969

AN EXPERIMENTAL EVALUATION OF PLASTICITY THEORIES FOR ANISOTROPIC METALS

by

R. M. W. Frederking[+] and O. M. Sidebottom[++]

ABSTRACT

An experimental investigation was undertaken to evaluate anisotropic plasticity theoreis which have been proposed in the literature. Three different metals in the form of 2.5 in. diameter bars were considered: SAE 1020 steel preloaded in tension to a strain of 8 percent, copper alloy 360 (free cutting brass) preloaded in tension to a strain of 3 percent, and 2024-T351 aluminum alloy as received. All metals had approximately the same properties in the radial and circumferential directions with greatly different properties in the axial direction. Tension and compression tests were conducted on specimens having directions of axial, circumferential and 45° to the axis. Hollow torsion tests were conducted on axial specimens. Biaxial tests were conducted on thin-walled cylinders. All loading was monotonic and proportionate and extended well into the plastic region.

The various anisotropic plasticity theories were evaluated by comparing theoretical and experimental yield curves for each material and by comparing theoretical load-deformation curves with experimentally determined curves for tension and compression specimens at 45° to the axis, for hollow torsion specimens, and for biaxial loading. In most cases good agreement was found between theory and experiment.

+ R. M. W. Frederking is Scientific Officer, Canadian Armament Research and Development Establishment, Quebec, Quebec, Canada.

++O. M. Sidebottom is Professor, Department of Theoretical and Applied Mechanics, University of Illinois, Urbana, Illinois.

NOTATION

r, θ, z	cylindrical coordinates
$\sigma_r, \sigma_\theta, \sigma_z, \tau_{\theta z}$	stress components
$d\epsilon_r^p, d\epsilon_\theta^p, d\epsilon_z^p, d\gamma_{\theta z}^p$	plastic strain increments for multiaxial states of stress
$d\epsilon_{\theta s}^p, d\epsilon_{zs}^p, d\gamma_{\theta zs}^p, d\epsilon_{\theta s}^{'p}, d\epsilon_{zs}^{'p}$	plastic strain increments for specimens used to obtain material properties
$\sigma = \sigma_{45}$	stress in specimen at 45^o to z axis
$d\epsilon^p$	incremental plastic strain in specimen at 45^o to z axis
Z, Z', T, T', S	values of yield stresses
F, G, H, L, M, N, Q, K	anisotropic parameters
$d\lambda$	proportionality scaling factor
E	Young's modulus
G	shearing modulus

INTRODUCTION

It is well known that many materials employed in engineering practice possess mechanical properties which are directionally dependent; these materials are termed anisotropic. Many investigators (1-13) either have proposed plasticity theories for anisotropic materials or have conducted experimental investigations to evaluate these theories. Two of the proposed theories will be presented later in the paper and will be compared with experimental data.

Plasticity theories for anisotropic materials require that both the yield condition and the loading function (or flow condition) be known for the material, these are empirically determined and are approximated by mathematical models. In addition stress-strain relations for the material are needed. The plasticity theories that have been proposed for anisotropic materials must also be valid for isotropic materials; the yield condition and stress-strain relations that have been proposed for anisotropic materials reduce to the von Mises yield condition and the Prandtl-Reuss stress-strain relations for isotropic materials.

Many of the experimental investigations have been concerned with the problem of evaluating the proposed yield conditions for anisotropic materials. The important design problem in the field of anisotropic plasticity is that of predicting load-deformation relations for load carrying members. This experimental investigation was undertaken to evaluate the various anisotropic theories in their ability to predict load-deformation relations for several load carrying members made of three different anisotropic metals.

STATEMENT OF PROBLEM

Three anisotropic metals were considered in the investigation. Preliminary tests indicated that radial and circumferential properties were nearly equal and are assumed to be identical. The yield condition for the anisotropic material can be investigated by obtaining material properties in the z, θ plane where z is in the axial direction and θ is in the circumferential direction.

The yield condition can be indicated by plotting the yield locus in the σ_z, σ_θ principal stress plane. Each material can be one of four Mises types as indicated in Fig. 1 by the yield locus, curve C, for the four materials. There are additional four types if the material approaches the Tresca yield condition instead of the von Mises yield condition. Many of the plasticity theories in the literature assume that the material is isotropic and even to give the von Mises yield condition which gives the ellipse for the σ_z, σ_θ plane in Fig. 1a. A material is even if a straight line through the origin intersect the yield locus at equal distances from the origin. Often in the literature an even material is referred to as a material with no Bauschinger effect.

Each of the three materials considered in the investigation was anisotropic and uneven as indicated in Fig. 1d. One of the problems considered in the investigation was to determine curve C for each material. Tension and compression specimens with axes parallel to the z axis gives points A and B, respectively, in Fig. 1. Similar specimens parallel to the θ axis gives points J and K. These data are sufficient for determining curve C in Fig. 1d for the anisotropic theories considered in the investigation. In addition to tension and compression data, hollow torsion data were obtained from specimens with axes parallel to the z axis. It should be noted that hollow torsion data do not give points on curve C in Fig. 1d. Curve C can be determined only by test members loaded so that the principal

stresses remain in the z and θ directions. Thin-walled cylinders subjected to axial load and internal pressure can be used to locate other points in the first quadrant in Fig. 1d. The other three quadrants can not be investigated using this member because of possibility of buckling. The theories that are available will be used to predict load-deformation relations for thin-walled cylinders subjected to proportionate loading to compare with experimental data for the three metals.

Theories also are available for predicting load-elongation diagrams for tension and compression specimens with axes inclined at an angle of 45^{o} to the z axis. These theories will be compared with experimental data. For principal axes at 45^{o} to the z axis, the yield curve C will be similar to that for an isotropic uneven material as indicated in Fig. 1b. Hollow torsion data from specimens with axis parallel to the z axis should give points L and M on this yield curve. The shape of this yield curve will be compared with that for the σ_z, σ_θ principal stress plane.

THEORY

The anisotropic theories that are presented later in this section are based on the following assumptions: 1. the material is homogeneous; 2. the material is elastically isotropic; 3. the material is plastically orthotropic; 4. the anisotropic parameters are variables which are dependent on the current level of the stresses; 5. the loading functions in the radial and circumferential directions are identical; and 6. all stress distributions are uniform.

In conducting tests of tension and compression specimens from the axial and circumferential directions, of hollow torsion specimens, and of thin-walled cylinders subjected to internal pressure and axial load, the nonzero stress components are σ_θ, σ_z, and $\tau_{\theta z}$. The yield conditions for the various anisotropic theories require two or more of the following yield stresses: tension and compression yield stresses, Z and $-Z'$, from axial specimens; tension and

compression yield stresses, T and -T', from circumferential specimens; and hollow torsion yield stress, S, from axially aligned torsion specimens. It should be noted that S could not be obtained from axial hollow torsion specimens unless radial and circumferential properties are identical.

Each anisotropic theory requires that three things be specified as follows: 1. a yield function; 2. stress-strain relations; and 3. a loading function.

Anisotropic Theory Proposed by Hill. Hill (1) was one of the earlier investigators of plastic anisotropy. He assumed that the material was anisotropic and even as indicated in Fig. 1c. His yield function has the form

$$2f(\sigma_{ij}) = F(\sigma_\theta - \sigma_z)^2 + G(\sigma_z - \sigma_r)^2 + H(\sigma_r - \sigma_\theta)^2 + 2L\tau_{\theta z}^2 + 2M\tau_{zr}^2 + 2N\tau_{r\theta}^2 = 1 \quad (1)$$

Multiaxial plasticity theories for isotropic and even materials that obey the von Mises flow condition usually uses the relation defining effective stress to relate the multiaxial stress components of the member to be analyzed to the stress components in the member used to obtain material properties. Equation 1 fulfills the same role for anisotropic materials that the effective stress relation does for isotropic and even materials. It should be noted that Eq. 1 reduces to the equation for effective stress for isotropic and even materials. Stress-strain relations for Hill's theory are given by the relation $d\epsilon_{ij}^p = d\lambda\, \partial f/\partial \sigma_{ij}$. In this investigation the nonzero stress components are σ_θ, σ_z, and $\tau_{\theta z}$. For these conditions the stress-strain relations simplify to

$$\begin{aligned} d\epsilon_z^p &= d\lambda \left[G\sigma_z + F(\sigma_z - \sigma_\theta)\right] \\ d\epsilon_\theta^p &= d\lambda \left[F(\sigma_\theta - \sigma_z) + H\sigma_\theta\right] \\ d\epsilon_r^p &= -d\lambda \left[G\sigma_z + H\sigma_\theta\right] \\ d\gamma_{\theta z}^p &= 2d\lambda\, L\tau_{\theta z} \end{aligned} \quad (2)$$

It will be noted that the first three of Eqs. 2 satisfie the condition that $d\epsilon_z^p + d\epsilon_\theta^p + d\epsilon_r^p = 0$. It will be noted also that the right side of the last of Eqs. 2

has the factor 2 which Hill does not have in his equations; the factor 2 arises from the fact that we are using the engineering definition of shearing strain, $\gamma_{\theta z}$, while Hill used the mathematically convenient definition equal to $\gamma_{\theta z}/2$. Equations 2 reduce to the Prandtl-Ruess stress-strain relations for isotropic and even materials.

For the condition that the nonzero stress components are σ_θ, σ_z, and $\tau_{\theta z}$, the anisotropic parameters in Eq. 1 simplify to

$$F = G = \frac{1}{2Z^2} \; ; \quad H = \frac{1}{T^2} - \frac{1}{2Z^2} \; ; \quad L = \frac{1}{2S^2} \tag{3}$$

Anisotropic Theory Proposed by Ota, Shindo, and Fukuoka. Ota, Shindo, and Fukuoka (2) assumed that the material was anisotropic and uneven (Fig. 1d). For the condition that the nonzero stress components are σ_θ, σ_z, and $\tau_{\theta z}$, their yield function takes the form

$$2f(\sigma_{ij}) = F(\sigma_\theta - \sigma_z)^2 + G\sigma_z^2 + H\sigma_\theta^2 - 2Q\sigma_z - 2R\sigma_\theta + 2L\tau_{\theta z}^2 = 1 \tag{4}$$

where (using absolute values for the yield stresses)

$$F = G = \frac{1}{2ZZ'} \; ; \quad H = \frac{1}{TT'} - \frac{1}{2ZZ'} \; ; \quad Q = \frac{Z - Z'}{2ZZ'} \; ; \quad R = \frac{T - T'}{2TT'} \; ; \quad L = \frac{1}{2S^2} \tag{5}$$

The stress-strain relations are

$$\begin{aligned} d\epsilon_z^p &= d\lambda \left[(F + G)\sigma_z - F\sigma_\theta - Q \right] \\ d\epsilon_\theta^p &= d\lambda \left[(F + H)\sigma_\theta - F\sigma_z - R \right] \\ d\gamma_{\theta z}^p &= 2d\lambda \, L\tau_{\theta z} \end{aligned} \tag{6}$$

Loading Function. The loading function is used to determine $d\lambda$ which in turn is used to determine values for the yield stresses for each increment of loading. Hill's theory will be considered since it includes fewer curves. Let the curves in Fig. 2 represent stress versus plastic strain for axial and circumferential

tension specimens and hollow torsion specimens. Relative values of Z, T, and S must satisfy the condition that $d\lambda$ in Eqs. 2 will be the same for the three specimens in Fig. 2. Thus,

$$d\lambda = Z\, d\epsilon^p_{zs} = T\, d\epsilon^p_{\theta s} = S\, d\gamma^p_{\theta zs} \tag{7}$$

where the subscript s distinguishes between plastic strain increments for specimens used to obtain material properties and the plastic strain increments in Eqs. 2. One of the curves in Fig. 2 is chosen to represent the loading function. If the curve for the circumferential specimen is chosen as the loading function, assume a value for $d\epsilon^p_{\theta s}$ to define both T and $d\lambda = T\, d\epsilon^p_{\theta s}$. Values of Z and S are obtained by trial and error solution of Eqs. 7 along with curves in Fig. 2. Sufficient accuracy is usually obtained by taking $d\epsilon^p_{zs} = d\epsilon^p_{\theta s}$ and $d\gamma^p_{\theta zs} = \sqrt{3}\ d\epsilon^p_{\theta s}$. It should be noted that Fig. 2 indicates only the first set of increments of the plastic strains. For the second set of increments and all subsequent set of increments of the plastic strains, values of T, Z, and S are defined as values of the stresses at the end of the plastic strain increments and Eqs. 7 must be satisfied for each set of increments of the plastic strains.

Theoretical Predictions for Thin-Walled Cylinders. Hill's theory for the thin-walled cylinders is presented since it is the simplest. Hill's theory for any given loading is obtained by using Eqs. 1, 2, 3, and 7 (with $d\lambda = T\, d\epsilon^p_{\theta s}$) along with curves of stress versus plastic strain for axial and circumferential tension specimens (see Fig. 2).

$\sigma_z = \sigma_\theta$. When thin-walled cylinders are loaded such that $\sigma_z = \sigma_\theta$, the following relations are obtained:

$$\sigma_z = \sigma_\theta = T$$

$$d\epsilon_z^p = \frac{T^2}{2Z^2}\, d\epsilon_{\theta s}^p \tag{8}$$

$$d\epsilon_\theta^p = d\epsilon_{\theta s}^p - d\epsilon_z^p$$

$\underline{\sigma_z = 2\sigma_\theta}$. Equations similar to Eqs. 8 can be derived for thin-walled cylinders loaded such that $\sigma_z = 2\sigma_\theta$.

$$\sigma_z = 2\sigma_\theta = \frac{2ZT}{\sqrt{2T^2 + Z^2}}$$

$$d\epsilon_z^p = \frac{3T\sigma_z}{4Z^2}\, d\epsilon_{\theta s}^p \tag{9}$$

$$d\epsilon_\theta^p = \frac{\sigma_z}{2T}\left[1 - \frac{T^2}{Z^2}\right] d\epsilon_{\theta s}^p$$

$\underline{\sigma_z = \sigma_\theta/2}$. For cylinders loaded such that $\sigma_z = \sigma_\theta/2$, the following relations are obtained:

$$\sigma_z = \frac{\sigma_\theta}{2} = \frac{ZT}{\sqrt{4Z^2 - T^2}}$$

$$d\epsilon_z^p = 0 \tag{10}$$

$$d\epsilon_\theta^p = \frac{T}{2\sigma_z}\, d\epsilon_{\theta s}^p$$

The first set of points on Hill's theoretical $\sigma_z - \epsilon_z$ and $\sigma_\theta - \epsilon_\theta$ diagrams for thin-walled cylinders are predicted by first assuming a value for $d\epsilon_{\theta s}^p$ to determine the magnitude of T as indicated in Fig. 2. Values of $d\epsilon_{zs}^p$ and Z are determined by satisfying Eq. 7. Substituting these in either Eqs. 8, 9, or 10 give values for σ_z, σ_θ, $d\epsilon_z^p$, and $d\epsilon_\theta^p$. Elastic components of the strains are given by Hooke's law. The second set of points on the diagrams were obtained by assuming

the next value for $d\epsilon^p_{\theta s}$ and repeating the calculation. The theoretical curves shown later in this paper were obtained by choosing values of $d\epsilon^p_{\theta s}$ equal to 0.0025, 0.0025, 0.0050, 0.0100, and 0.0100 to cover a range of $\epsilon^p_{\theta s}$ equal to 0.0300.

Similar theoretical curves can be obtained based on Ota, Shindo, and Fukuoka's theory. Their theory is obtained using Eqs. 4, 5, 6, and 7 ($d\lambda = T\, d\epsilon^p_{\theta s} = T'\, d\epsilon'^p_{\theta s} = Z\, d\epsilon^p_{zs} = Z'\, d\epsilon'^p_{zs}$) along with curves of stress versus plastic strain for axial and circumferential tension and compression specimens.

Theoretical Predictions for Tension and Compression Specimens at 45^o to the z axis. Consider a tension specimen whose axis makes an angle ϕ with respect to the z axis. If the stress in this specimen is designated as σ, then equilibrium requires that $\sigma_z = \sigma \cos^2\phi$, $\sigma_\theta = \sigma \sin^2\phi$, and $\tau_{\theta z} = \sigma \sin\phi \cos\phi$. These stress components can be substituted in Eqs. 1 and 2 for Hill's theory which gives for $\phi = 45^o$

$$\sigma = \frac{2}{\sqrt{G + H + 2L}} \tag{11}$$

and

$$\begin{aligned} d\epsilon^p_z &= \frac{\sigma}{2} G\, d\lambda = \frac{\sigma}{2} G\, T\, d\epsilon^p_{\theta s} \\ d\epsilon^p_\theta &= \frac{\sigma}{2} H\, d\lambda = \frac{\sigma}{2} H\, T\, d\epsilon^p_{\theta s} \\ d\gamma^p_{\theta z} &= \sigma\, L\, d\lambda = \sigma\, L\, T\, d\epsilon^p_{\theta s} \end{aligned} \tag{12}$$

where $d\lambda = T\, d\epsilon^p_{\theta s}$ as indicated by Eq. 7. The yield stresses Z, T, and S are needed to determine G, H, and L are obtained by a trial and error solution of Eqs. 7 along with plots of stress versus plastic strain for axial and circumferential tension specimens and hollow torsion specimens (see Fig. 2). The plastic strain increment $d\epsilon^p$ for the tension specimen at 45^o can be obtained from the geometry of deformation as

$$d\epsilon^p = \frac{d\epsilon_z^p}{2} + \frac{d\epsilon_\theta^p}{2} + \frac{d\gamma_{\theta z}^p}{2} \tag{13}$$

Equations 11, 12, and 13 give

$$d\epsilon^p = \frac{\sigma}{4}(G + H + 2L)\, T\, d\epsilon_{\theta s}^p = \frac{T}{\sigma}\, d\epsilon_{\theta s}^p \tag{14}$$

The first point on the stress-strain diagram at 45^o to the z axis is given by the stress σ and the strain $\epsilon = d\epsilon^p + \sigma/E$. Other points are calculated by repeating the procedure. The same procedure is used to predict the stress-strain diagram for compression specimens at 45^o to the z axis. In this case the yield stresses Z', T', and S needed to determine G, H, and L are obtained from plots of stress versus plastic strain for axial and circumferential compression specimens and hollow torsion specimens.

The theory of Ota, Shindo, and Fukuoka can also be used to predict stress-strain diagrams for specimens at 45^o to the z axis. Their theory requires plots of stress versus plastic strain for axial and circumferential tension and compression specimens and hollow torsion specimens. The number of calculations for their theory is appreciably greater than for Hill's theory. Identical stress-strain curves are predicted for tension and compression specimens at 45^o to the z axis. Since this curve is in close agreement with the average of the two curves predicted by Hill's theory, the curve predicted by the Ota, Shindo, and Fukuoka's theory is not presented.

Theoretical Prediction for Hollow Torsion Specimens. The principal stress directions for the hollow torsion specimens are identical with tension and compression specimens taken at 45^o to the z axis. The data for the tension and compression specimens were nearly identical so that Hill's theory approaches the von Mises ellipse for these principal directions. Let the $\sigma - \epsilon$ diagram be the average stress-strain diagram obtained from the tension and compression data, then

$$\tau_{\theta z} = \frac{\sigma}{\sqrt{3}} \tag{15}$$

and

$$d\gamma^{p}_{\theta z} = \sqrt{3}\ d\epsilon^{p} \tag{16}$$

The $\tau_{\theta z} - \gamma_{\theta z}$ diagram is predicted using Eqs. 15 and 16 and the elastic constants for the material.

MATERIALS AND EXPERIMENTAL PROCEDURES

Three materials were tested as follows: SAE 1020 steel, copper alloy 360 (0.615 Cu., 0.355 Zn., and 0.03 Pb.) and 2024-T351 aluminum alloy. Each material was purchased as 2.5 in. diameter bars. The anisotropy of the steel and brass was increased by preloading; the steel bar was given a permanent set in tension of 8 percent while the brass bar was given a permanent set of about 3 percent when it necked and broke near one of the grips. The Bauschinger effect is known to be time dependent after plastic deformation; the time dependence was assumed to be removed by aging the steel at room temperature for two weeks and by aging the brass at 400^{o} F for 24 hours.

The thin-walled cylinders had an inside diameter of 1.790 in., a wall thickness of 0.050 in. $\pm$ 0.0005 in., a length of 6.5 in., and a constant thickness length of 5.5 in. An attempt was made to have the center lines of each of the tension, compression, and hollow torsion specimens located at the same radius in the 2.5 in. diameter bar as the wall of the thin-walled cylinders. This was physically impossible in all cases. The tension and compression specimens had a length of 1.75 in. and a diameter of 0.375 in., the reduced section for the tension specimens was 0.150 in. The hollow torsion specimens had an outside diameter of 0.600 in. and an inside diameter of 0.500 in.

All test members were loaded at a sufficiently slow rate of loading that the time effects could be considered to be negligible. The tension and compression specimens were loaded in a 10,000 lb capacity testing machine; the strains were measured using a 1 in. clip gage. The hollow torsion specimens were loaded using a pendulum type torsion machine; the angle of twist was measured over a 2 in. gage length. The axial load for the thin-walled cylinders was applied by a 120,000 lb capacity testing machine while the internal pressure was produced by a simple ram loaded in compression in a 10,000 lb capacity testing machine. Water was used as the pressurizing fluid. The test fixture is shown in Fig. 3. The axial strains were measured by a clip gage over a 4 in. gage length. The circumferential strains were measured by taking the average of two clip gages that measured changes in diameter of the cylinder on perpendicular diameters.

The elastic constants for the three materials were found to be $E = 30,200,000$ psi and $G = 11,400,000$ psi for the SAE 1020 steel, $E = 14,400,000$ psi and $G = 5,100,000$ psi for copper alloy 360, and $E = 10,000,000$ psi and $G = 3,860,000$ psi for the 2024-T351 aluminum alloy.

ANALYSIS OF DATA

Tension and Compression Data. A series of tension specimens machined from various radii across the 2.5 in. diameter indicated that the yield stress for the SAE 1020 steel and the brass varied with the radius; however, the shape of the stress-strain diagram was not influenced by radial location. The center line of several specimens were not located at the same location as the wall of the thin-walled cylinders; the yield stresses for these specimens were adjusted by extrapolation.

Tension and compression stress-strain data for axial and circumferential specimens and from specimens whose axes made an angle of 45° with the z axis

are shown in Fig. 4 for SAE 1020 steel, in Fig. 5 for copper alloy 360 (free cutting brass), and in Fig. 6 for 2024-T351 aluminum alloy. The data points shown for a given type of specimen represent the average of data points for several specimens taken at various locations along the bar. All of the stress-strain diagrams for a given type of specimen had the same shape; however, considerable scatter was observed for the yield stresses. The greatest scatter of plus or minus 8 percent was observed for axial tension specimens of SAE 1020 steel; the maximum scatter for other speciemsn was plus or minus 4 percent.

The data in Figs. 4, 5, and 6 indicate that the three metals were anisotropic. The anisotropy was the most pronounced for the SAE 1020 steel and the 2024-T351 aluminum alloy.

Tension and compression data for specimens at 45^{o} to the z axis are indicated by the upper test points in Figs. 4, 5, and 6. The solid and dashed curves are the predicted tension and compression stress-strain diagrams, respectively, for these specimens using Hill's theory. The theory was obtained using Eqs. 11 through 14, the appropriate data in Figs. 4, 5, and 6 and the hollow torsion data (see Fig. 10). It will be noted that good agreement was found between theory and experiment in all cases.

Yield Curves. The stress-strain data in Figs. 4, 5, and 6 indicate that the stress that initiates yielding in some of the specimens was difficult to determine. Instead of presenting the initial yield curve for each material, each yield curve in Figs. 7, 8, and 9 represents the stress that will initiate yielding when the plastic strain is 0.0025.

In each of Figs. 7, 8, and 9 the yield curve was determined for both the σ_z, σ_θ principal stress plane and for the σ_{45}, σ_{45} principal stress plane. These elliptically shaped curves represents Ota, Shindo, and Fukuoka's theory which passes through the four points represented by the tension (open circles) and

compression (closed circles) data. The two sets of principal stress axes are translated and rotated with respect to each other in order to allign the two elliptically shaped curves so that their shapes can be compared. It will be noted that good agreement was found between the two yield curves. The torsion data indicated by open triangles should fall on the dashed curve in each case. Here again good agreement was found between theory and experiment. The thin-walled cylinder data indicated by open squares should fall on the solid curve in each case. The agreement between the theory and the biaxial test data was good in some cases but poor in other cases.

Hill's theory assumes that each material is even, i.e. the tension and compression stress-strain diagrams for a given direction are identical, (see Fig. 1c). The two yield curves for Hill's theory indicated greater difference than was the case for Ota, Shindo, and Fukuoka's theory.

Torsion Data. Test data was obtained for two hollow torsion specimens of each material and are plotted in Fig. 10. The solid curve in each case is the theory based on the average of the tension and compression data for specimens at 45^{o} to the z axis. Good agreement is noted between theory and experiment. Only in the case of 2024-T351 aluminum alloy was the theory nonconservative.

Thin-Walled Cylinder Data. Test data were obtained for two cylinders each of SAE 1020 steel (Fig. 11), of copper alloy 360 (Fig. 12), and of 2024-T351 aluminum alloy (Fig. 13) subjected to loading such that $\sigma_z = \sigma_\theta$. In addition one cylinder each of 2024-T351 aluminum alloy was subjected to loading such that $\sigma_z = 2\sigma_\theta$ and $2\sigma_z = \sigma_\theta$; these data are shown in Fig. 14.

Data for the two cylinders in each of Figs. 11,12, and 13 indicate good reproducibility of data. The solid and dashed curves in these figures are theoretical $\sigma_z - \epsilon_z$ and $\sigma_\theta - \epsilon_\theta$ curves, respectively, predicted using Hill's theory; the theory was predicted using Eqs. 2, 3, 7, and 8. Similar theoretical curves were predicted

using Ota, Shindo, and Fukuoka's theory and are shown in Figs. 11, 12 and 13 as dash-dot and dotted curves. The theory by Ota, Shindo, and Fukuoda more accurately predicted the strains particularly for small plastic strains. The discrepancy between their theory and experiment was not large except for the cylinders made of copper alloy 360. Hill's theory more accurately predicted the general shape of the axial and circumferential stress-strain curves; his theory was conservative in all cases.

The data for the two cylinders in Fig. 14 show the effect of the anisotropy of the 2024-T351 aluminum alloy. As indicated in Fig. 6, this material has much greater strength in the axial direction than in the circumferential direction. The cylinder loaded such that $\sigma_z = 2\sigma_\theta$ exhibited greater strength than the cylinder loaded such that $2\sigma_z = \sigma_\theta$. Theoretical curves are shown in Fig. 14 for both Hill's theory and the theory by Ota, Shindo, and Fukuoka. It will be noted that the theoretical curves are nonconservative for these cylinders.

Why should theories that are conservative for cylinders that are loaded so that $\sigma_\theta = \sigma_z$ be nonconservative for cylinders loaded so that either $\sigma_\theta = 2\sigma_z$ or $2\sigma_\theta = \sigma_z$? First, it should be noted that this result was obtained only for one of the three metals investigated and may not have been found for the other two metals. Second, it should be noted that, assuming hydrostatic states of stress do not influence plastic deformations, the state of stress in cylinders loaded so that $\sigma_\theta = \sigma_z$ is the same as for a uniaxial state of stress while the state of stress in cylinders loaded so that either $\sigma_\theta = 2\sigma_z$ or $2\sigma_\theta = \sigma_z$ is the same as for pure shear state of stress. The flow condition used in this investigation reduces to the von Mises flow condition for isotropic and even materials. Theories based on the von Mises flow condition are nonconservative in predicting the deformations of members if the state of stress is pure shear and if the material lies between a von Mises

material and a Tresca material. As indicated in Fig. 10, the 2024-T351 aluminum alloy was the only one of the three metals for which pure shear data fell below the theory.

CONCLUSIONS

An experimental investigation was undertaken to evaluate anisotropic plasticity theories. Three anisotropic metals were considered: SAE 1020 steel prestrained in tension to 8 percent, copper alloy 360 (free cutting brass) prestrained in tension 3 percent, and as received 2024-T351 aluminum alloy. These metals were purchased as 2.5 in. diameter bars. Preliminary tests indicated that radial and circumferential properties were nearly the same and were assumed to be identical. Tests included tension and compression loading of specimens from axial, circumferential, and 45^{o} to axial directions, hollow torsion loading of axial specimens, and biaxial loading of thin-walled cylinders.

Two anisotropic plasticity theories were considered as follows: Hill's theory and Ota, Shindo, and Fukuoka's theory. The theory of Ota, Shindo, and Fukuoka did a better job of representing the yield function for a given material than did the theory by Hill since all anisotropic metals are uneven (different properties in tension and compression) and Hill's theory assumes that the material is even. The reason for having an anisotropic plasticity theory is to predict load-deformation relations for load carrying members. For most of the members considered in this investigation, the theory by Ota, Shindo, and Fukuoka more accurately predicted the load-deformation relations. In almost all cases Hill's theory was more conservative than the theory by Ota, Shindo, and Fukuoka. Of the two theories, Hill's theory was much easier to apply.

The intersection of yield functions with both the σ_z, σ_θ and the σ_{45}, σ_{45} principal stress planes were obtained for each metal. The two yield curves for each metal were found to have approximately the same elliptical shape, however, the two curves had different displacements and rotations relative to the principal axes.

REFERENCES

1. R. Hill, "Mathematical Theory of Plasticity," Oxford University Press, 1950.

2. T. Ota, A. Shindo, and H. Fukuoka, "A Consideration on Anisotropic Yield Criterion," Proceedings of the 9th Japan National Congress for Applied Mechanics, p. 117, 1959.

3. I. I. Gol'denblat and V. A. Kopnov, "Strength Criteria for Anisotropic Materials," Izv. A. N. SSSR., Mekh., No. 6, p. 77, 1965.

4. R. Edelman and D. C. Drucker, "Some Extensions of Elementary Plasticity Theory," J. Franklin Inst., Vol. 251, No. 6, p. 581, 1951.

5. A. Zukuv, "Strength and Plasticity of Alloy D16T Under Complex Loading State," (in Russian), Izv. A. N. SSSR, Otdl. Tech. Nauk., No. 6, p. 61, 1954.

6. L. W. Hu and J. Marin, "Anisotropic Loading Functions for Combined Stresses in the Plastic Range," J. Appl. Mech., Vol. 22, No. 1, p. 77, 1955.

7. L. W. Hu, "Studies on Plastic Flow of Anisotropic Metals," J. Appl. Mech., Vol. 23, p. 444, 1956.

8. J. Olszak and W. Urbanowski, "The Plastic Potential and the Generalized Distortion Energy in the Theory of Non-Homogeneous Anisotropic Elastic-Plastic Bodies," Arch. Mech. Stos., Vol. 8, p. 671, 1956.

9. I. Berman and P. G. Hodge, "A General Theory of Piecewise Linear Plasticity for Initially Anisotropic Materials," Arch. Mech. Stos., Vol. 11, No. 5, p. 513, 1959.

10. A. Sawczuk, "Linear Theory of Plasticity of Anisotropic Bodies and Its Applications to Problems of Limit Analysis," Arch. Mech. Stos., Vol. 11, No. 5, p. 541, 1959.

11. A Baltov and A. Sawczuk, "A Rule for Anisotropic Hardening,", Mekhanica, Vol. 1, No. 2, p. 81, 1965.

12. N. L. Svensson, "Anisotropy and the Bauschinger Effect in Cold Rolled Aluminum," J. M. E. S., Vol. 8, No. 2, p. 162, 1966.

13. W. R. Jensen, W. E. Falby, and N. Prince, "Matrix Analysis Methods for Anisotropic Inelastic Structures," AFFDL-TR-65-220, (AD 486-295).

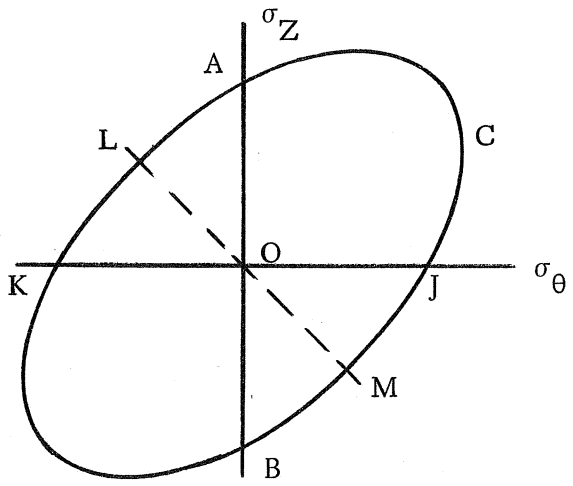

(a) ISOTROPIC EVEN

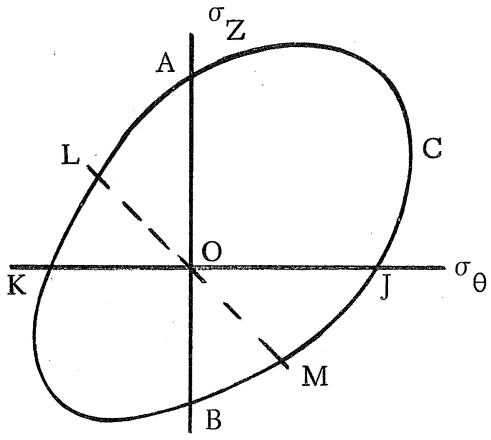

(b) ISOTROPIC UNEVEN

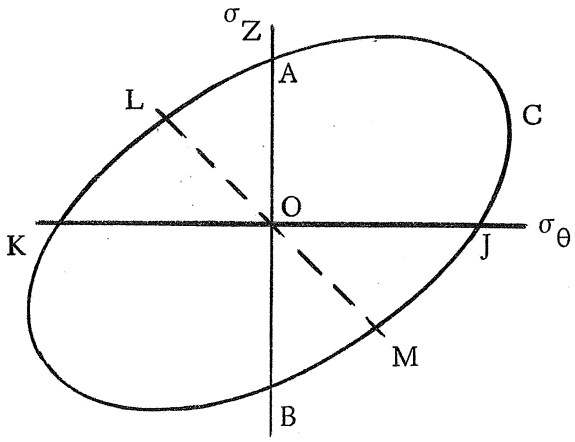

(c) ANISOTROPIC EVEN

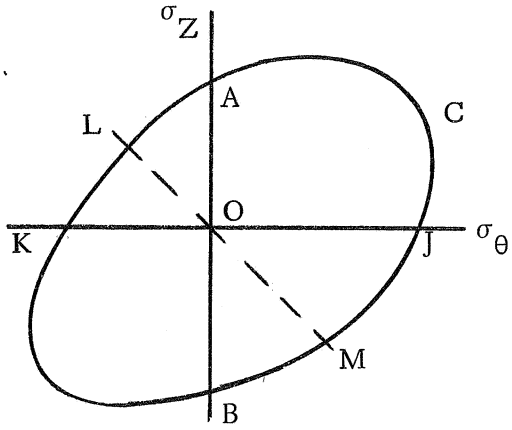

(d) ANISOTROPIC UNEVEN

Fig. 1. Yield Curves for Four Materials

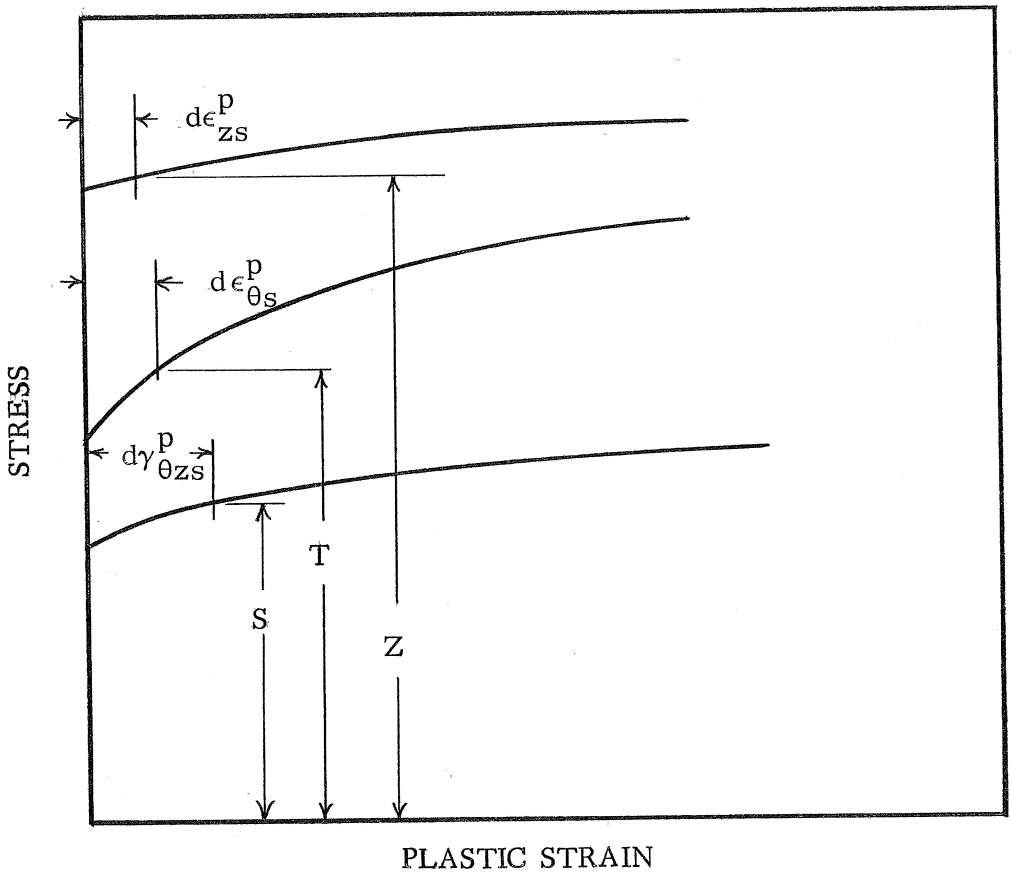

Fig. 2. Loading Function for Hill's Theory

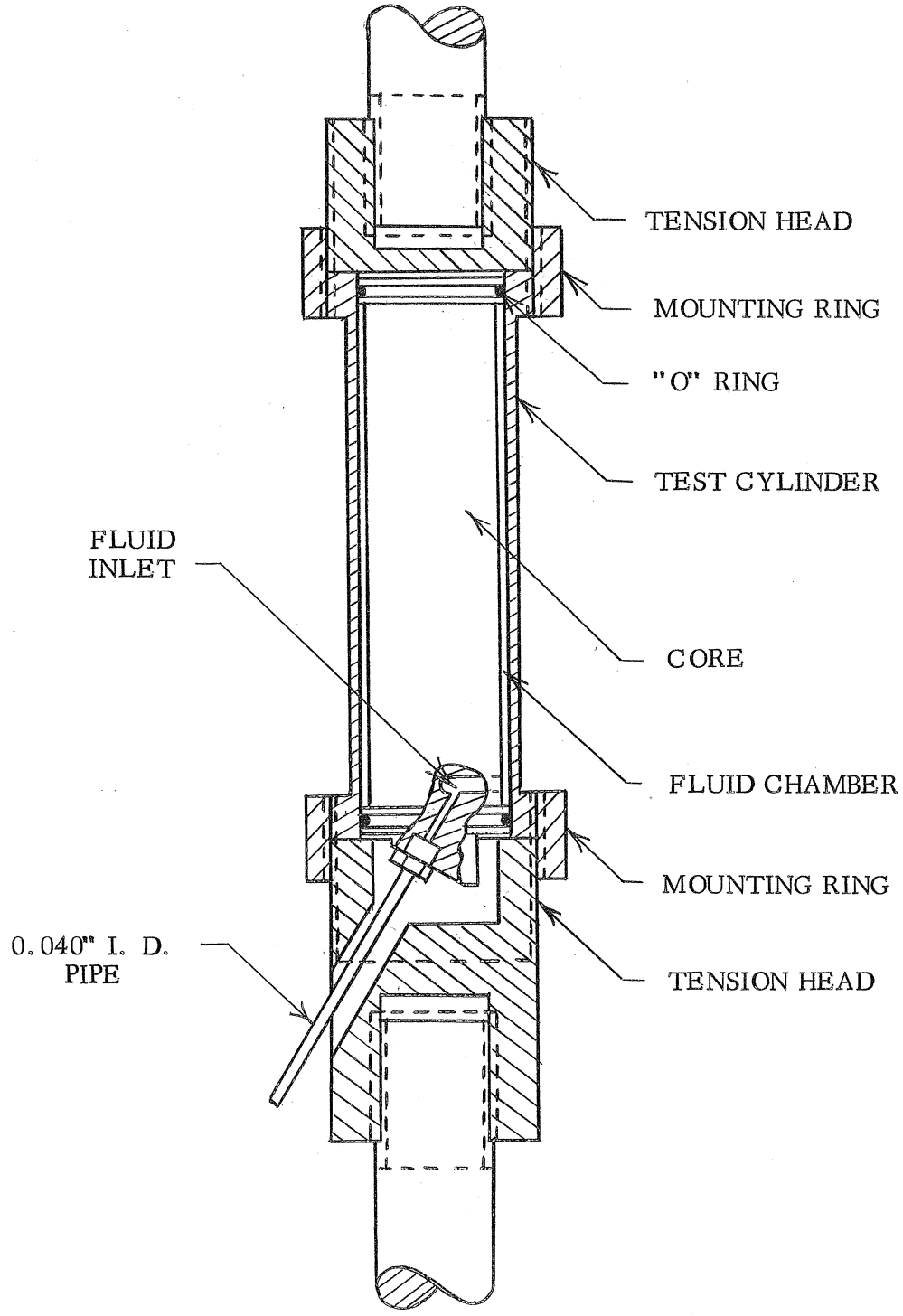

Fig. 3. Loading Fixture

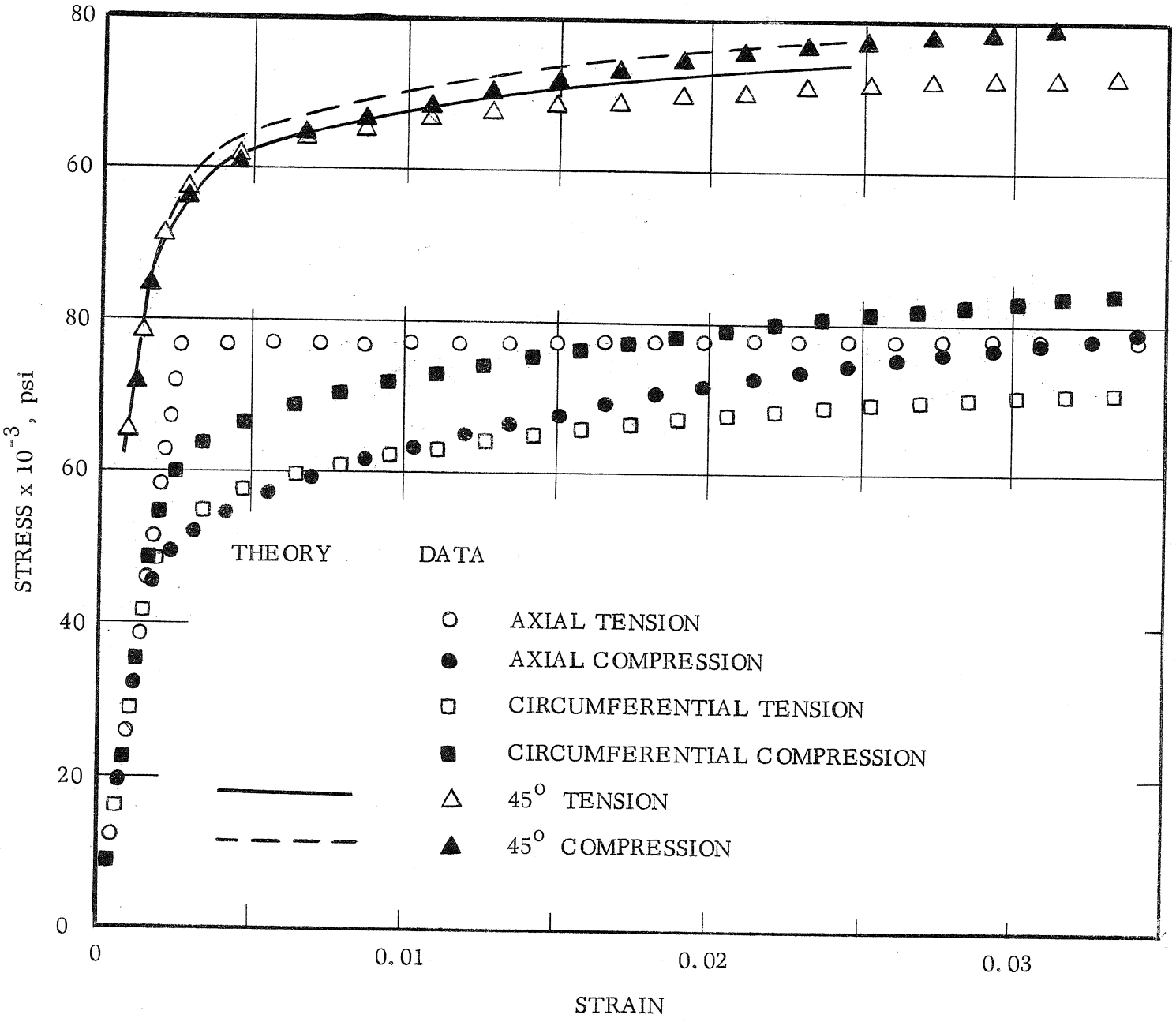

Fig. 4. Stress-Strain Diagrams for SAE 1020 Steel

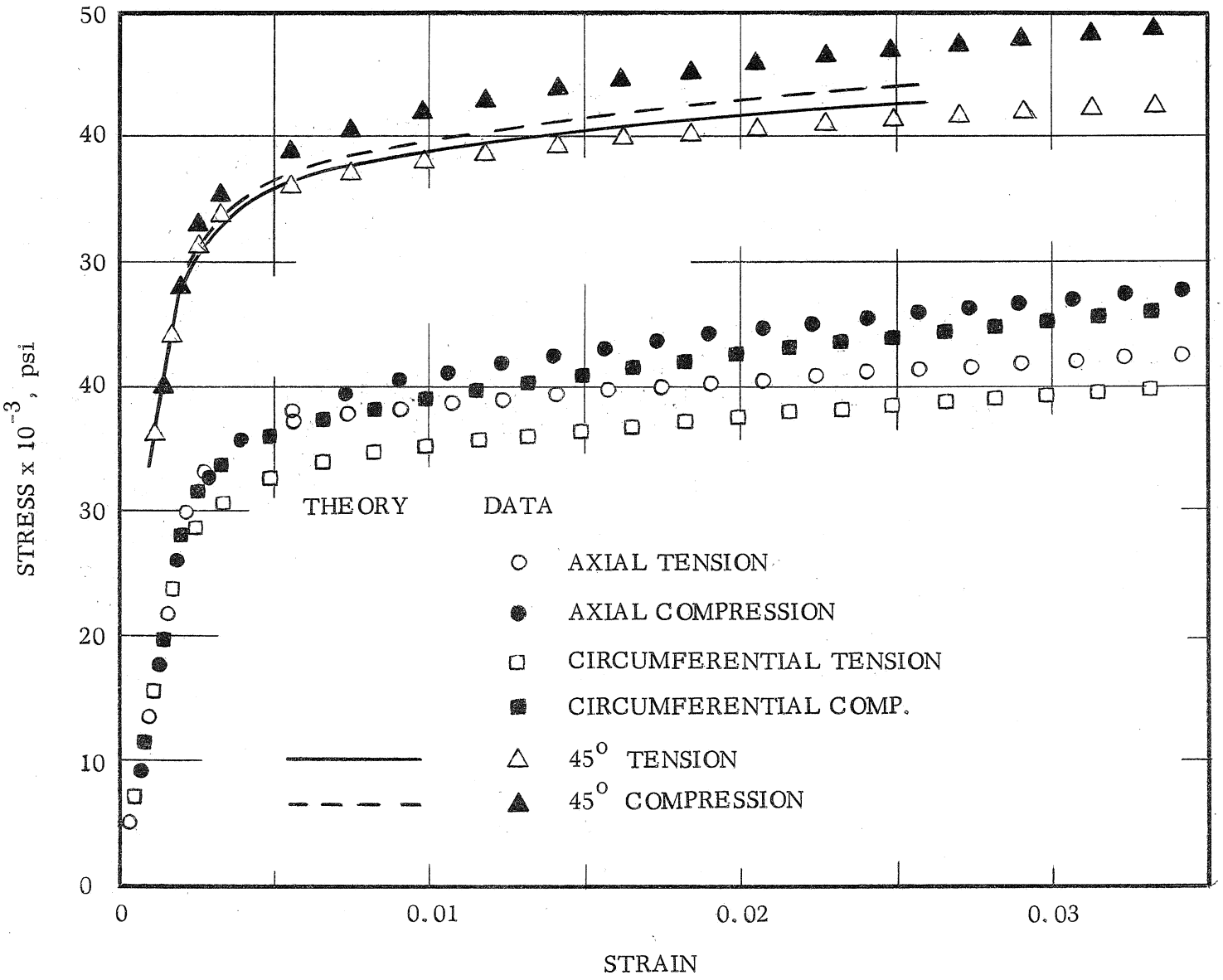

Fig. 5. Stress-Strain Diagrams for Copper Alloy 360, Free Cutting Brass

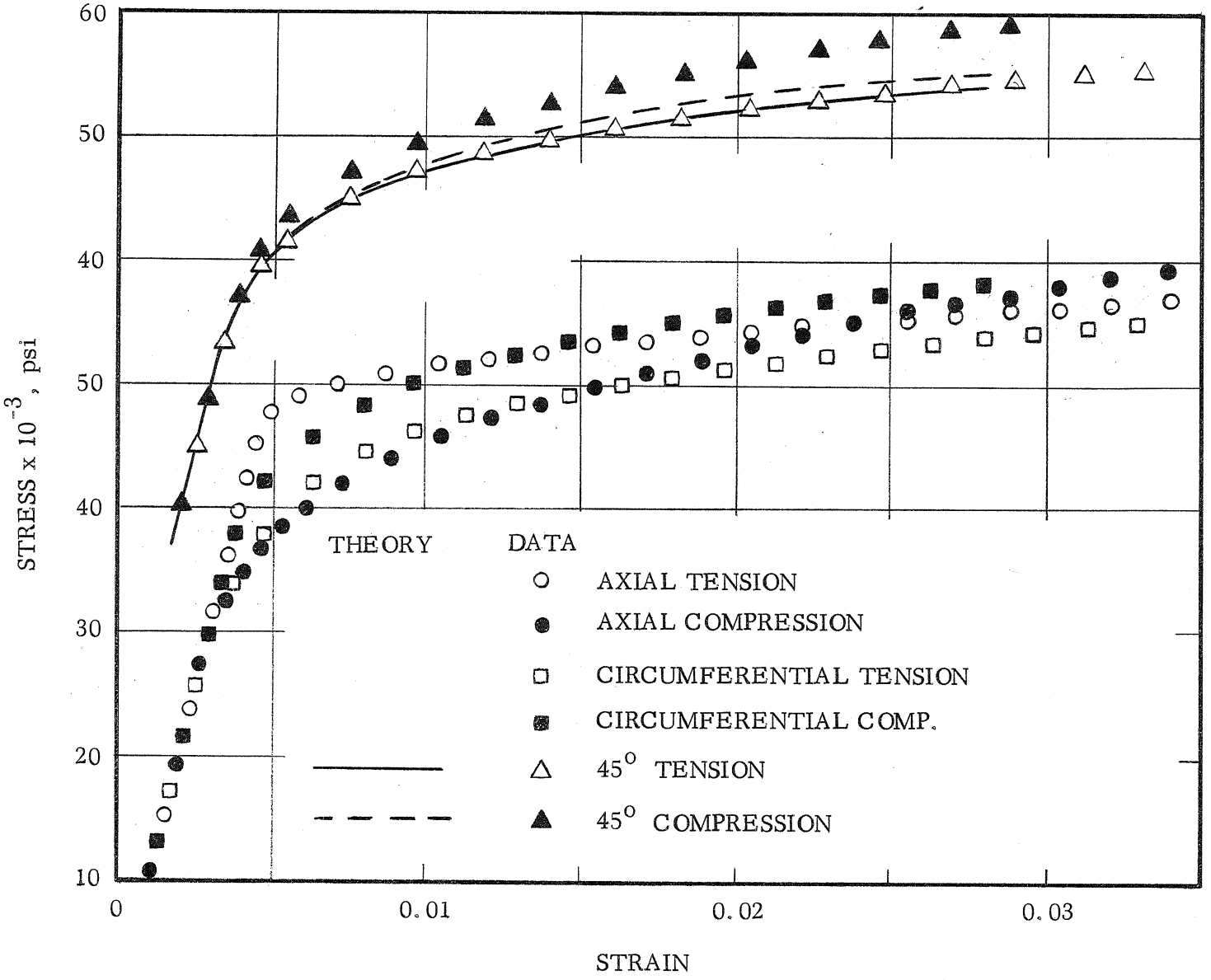

Fig. 6. Stress-Strain Diagrams for 2024-T351 Aluminum Alloy

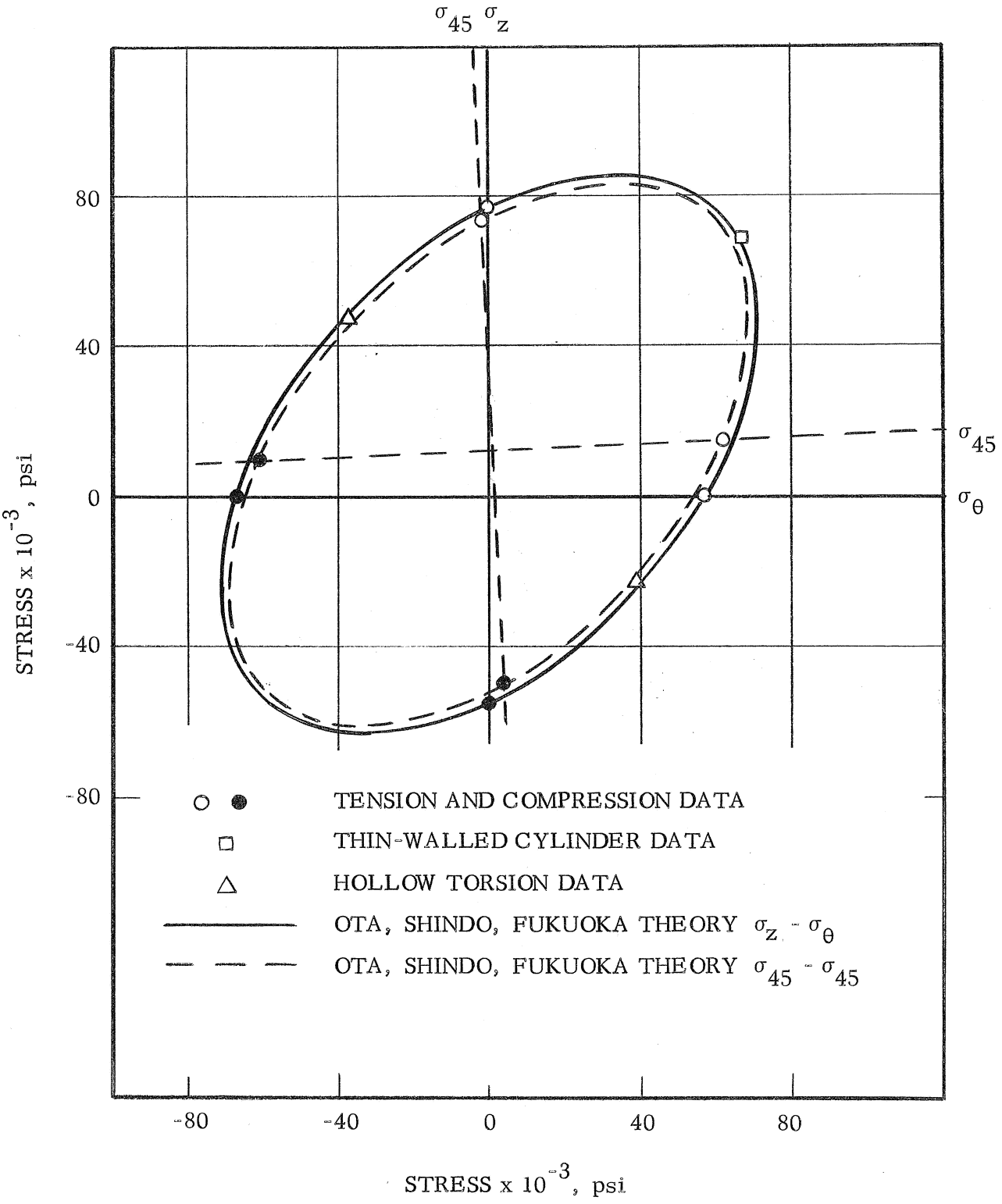

Fig. 7. Yield Curves for the σ_z, σ_θ and σ_{45}, σ_{45} Principal Stress Planes - SAE 1020 Steel

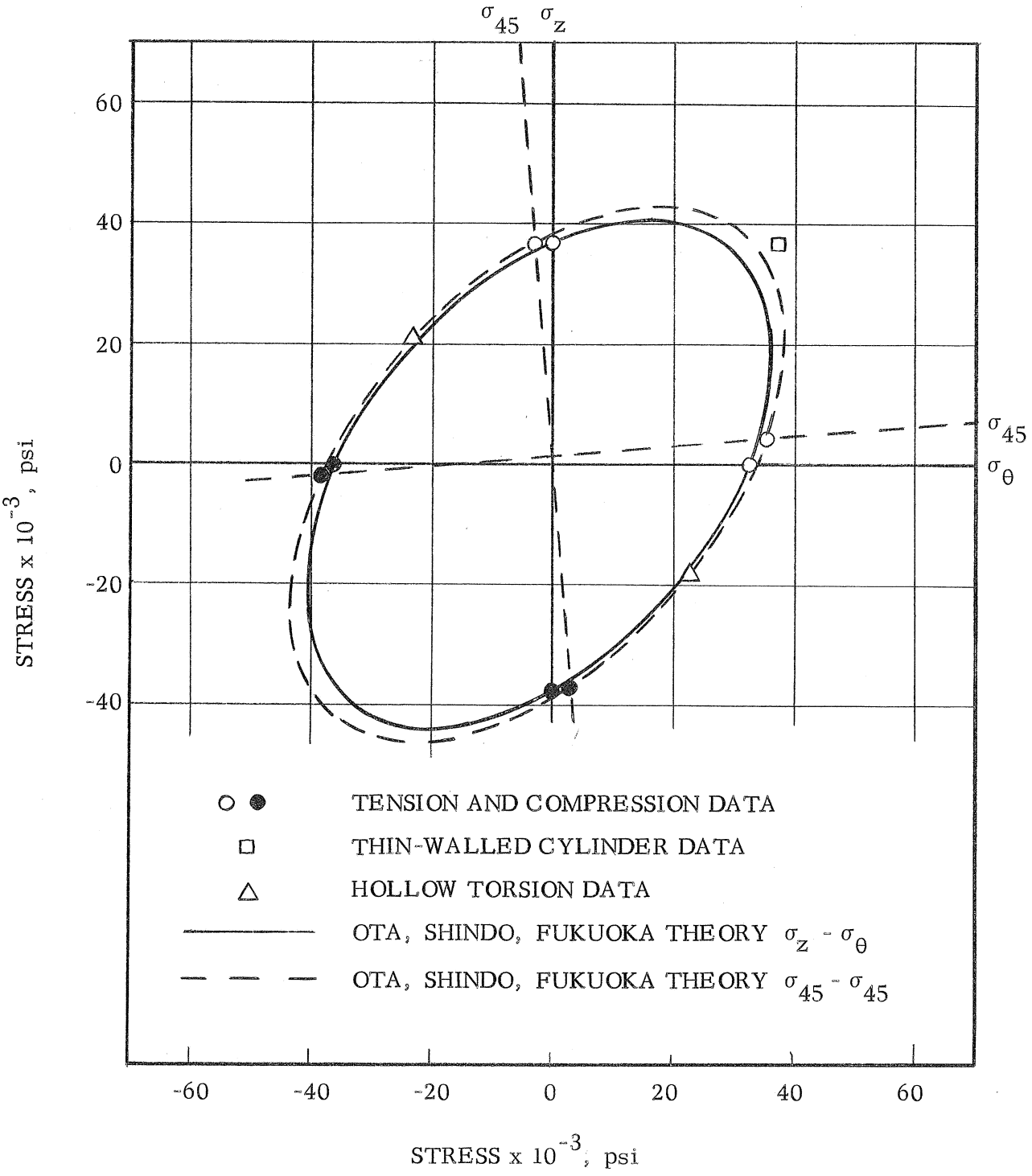

Fig. 8. Yield Curves for the σ_z, σ_θ and σ_{45}, σ_{45} Principal Stress Planes - Copper Alloy 360

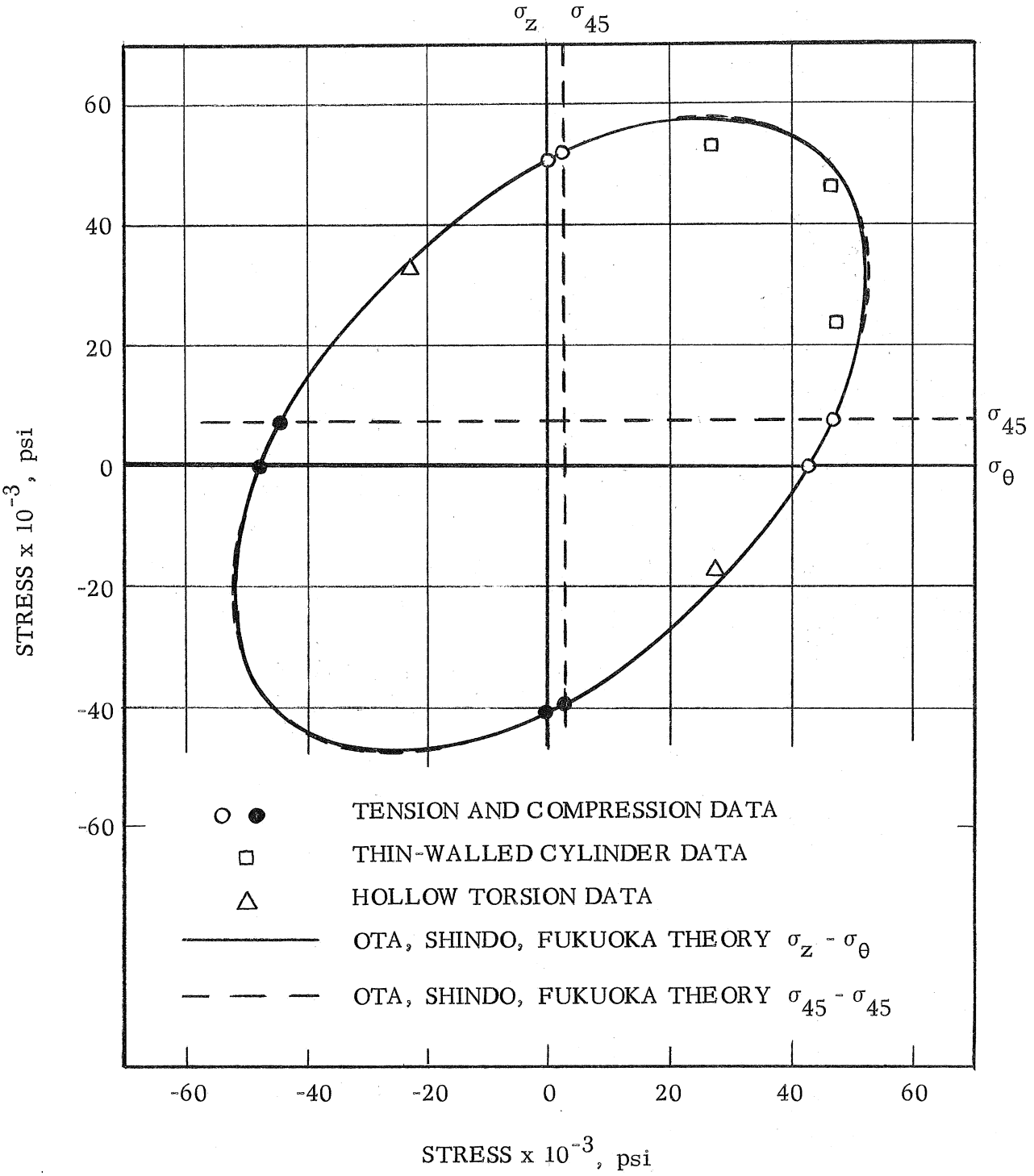

Fig. 9. Yield Curves for the σ_z, σ_θ and σ_{45}, σ_{45} Principal Stress Planes - 2024-T351 Aluminum Alloy

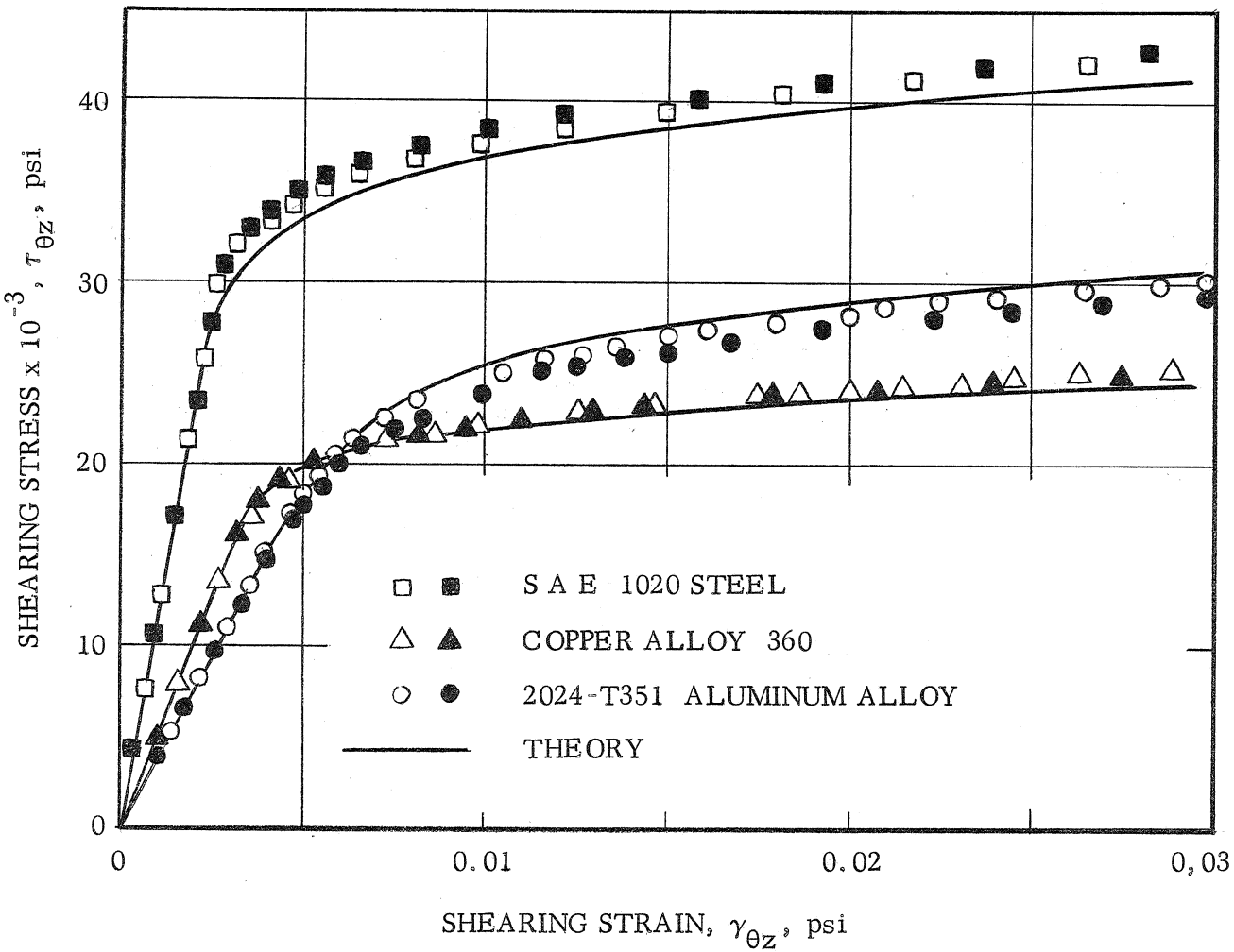

Fig. 10. Shearing Stress-Shearing Strain Diagrams

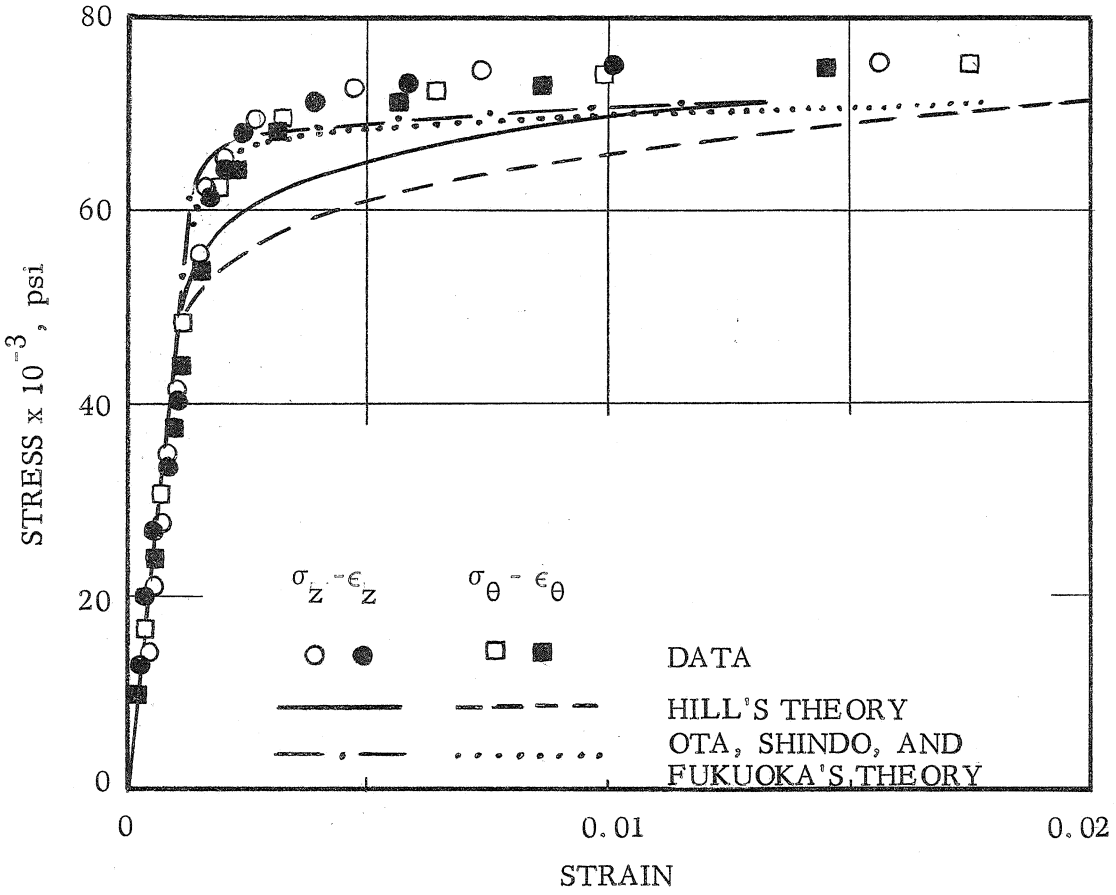

Fig. 11. Biaxial Loading ($\sigma_z = \sigma_\theta$) of Thin-Walled Cylinders Made of SAE 1020 Steel

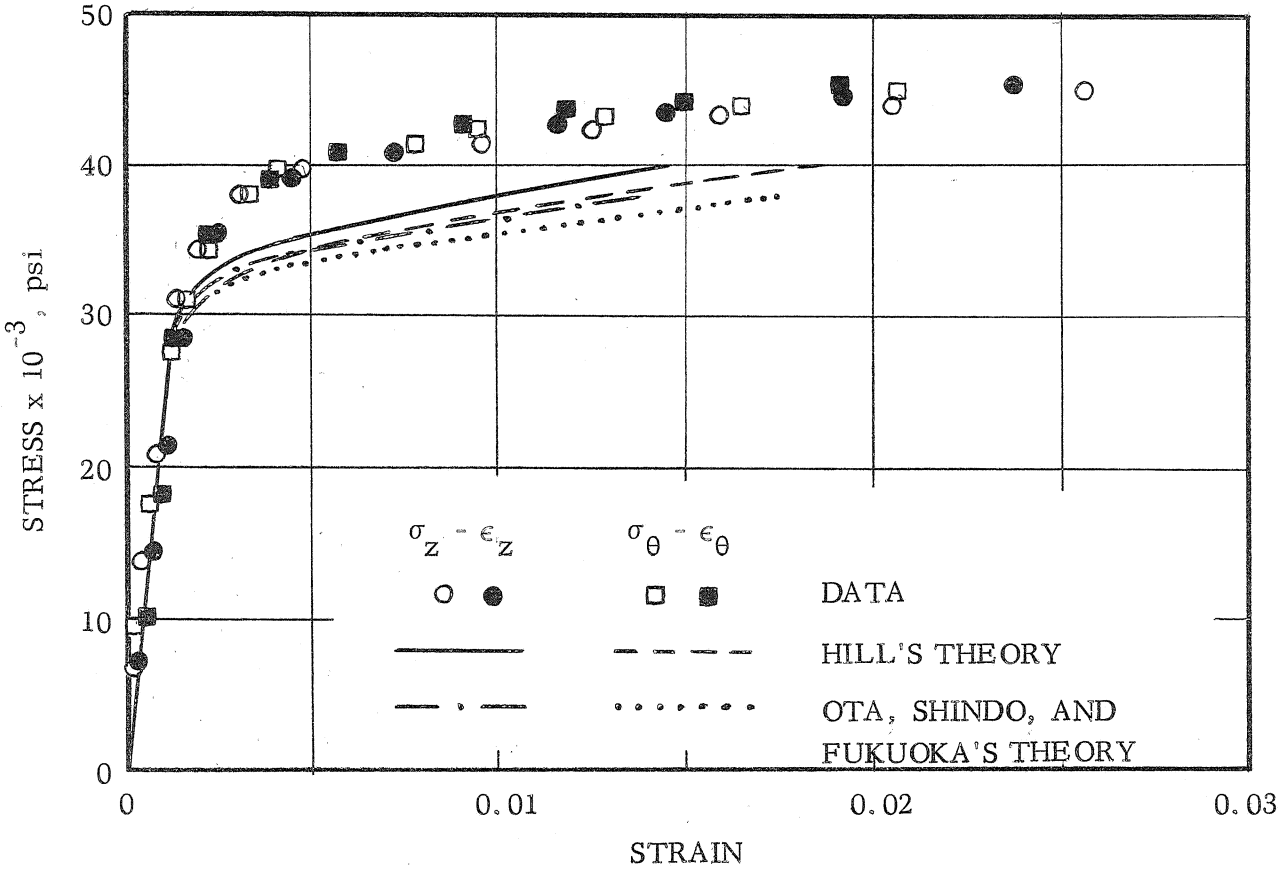

Fig. 12. Biaxial Loading ($\sigma_z = \sigma_\theta$) of Thin-Walled Cylinders Made of Copper Alloy 360

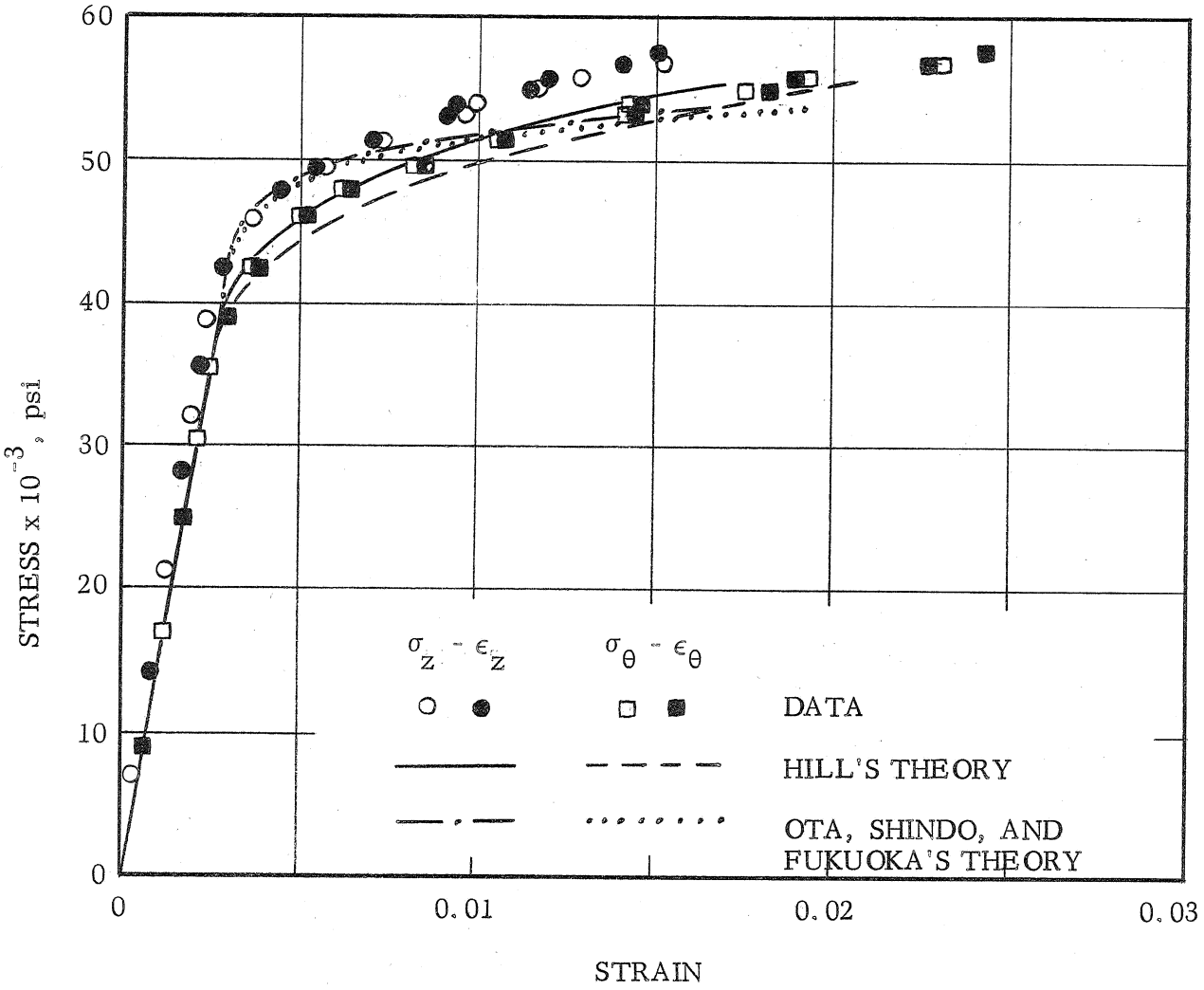

Fig. 13. Biaxial Loading ($\sigma_z = \sigma_\theta$) of Thin-Walled Cylinders Made of 2024-T351 Aluminum Alloy

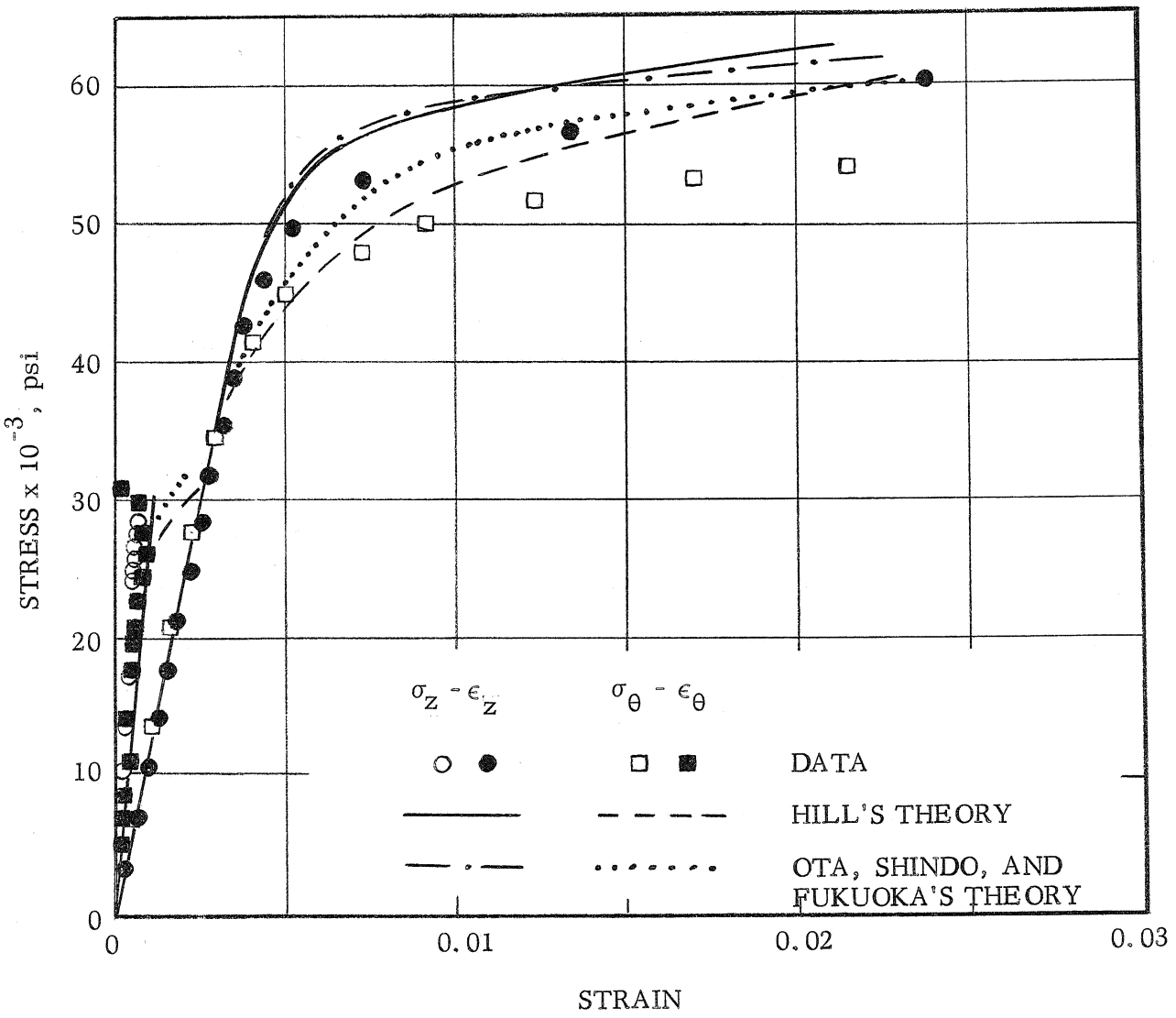

Fig. 14. Biaxial Loading ($\sigma_z = 2\sigma_\theta$ and $2\sigma_z = \sigma_\theta$) of Thin-Walled Cylinders Made of 2024-T351 Aluminum Alloy